IOP Publishing Journal of Physics: Condensed Matter
J. Phys.: Condens. Matter **26** (2014) 394007 (6pp) doi:10.1088/0953-8984/26/39/394007

Magnon dispersion in thin magnetic films

T Balashov[1], P Buczek[2], L Sandratskii[2], A Ernst[2,3] and W Wulfhekel[1]

[1] Physikalisches Institut, Karlsruhe Institute of Technology, Wolfgang-Gaede Strasse 1, 76131 Karlsruhe, Germany
[2] Max-Planck-Institut für Mikrostrukturphysik, Weinberg 2, 06120 Halle, Germany
[3] Wilhelm-Ostwald-Institut für Physikalische und Theoretische Chemie, Universität Leipzig, Linnéstraße 2, 04103 Leipzig, Germany

E-mail: Timofey.Balashov@kit.edu

Received 28 April 2014, revised 4 July 2014
Accepted for publication 29 July 2014
Published 12 September 2014

Abstract

Although the dispersion of magnons has been measured in many bulk materials, few studies deal with the changes in the dispersion when the material is in the form of a thin film, a system that is of interest for applications. Here we review inelastic tunneling spectroscopy studies of magnon dispersion in Mn/Cu_3Au(1 0 0) and present new studies on Co and Ni thin films on Cu(1 0 0). The dispersion in Mn and Co films closely follows the dispersion of bulk samples with negligible dependence on thickness. The lifetime of magnons depends slightly on film thickness, and decreases considerably as the magnon energy increases. In Ni/Cu(1 0 0) films the thickness dependence of dispersion is much more pronounced. The measurements indicate a considerable mode softening for thinner films. Magnon lifetimes decrease dramatically near the edge of the Brillouin zone due to a close proximity of the Stoner continuum. The experimental study is supported by first-principles calculations.

Keywords: magnetic thin films, magnons, inelastic tunneling spectroscopy

(Some figures may appear in colour only in the online journal)

Magnons in thin films and nanostructures play an important role in the description of the high-frequency dynamics of magnetic elements in spintronic devices. Magnetization dynamics on the nanoscale has e.g. been measured with ferromagnetic resonance, which requires the signal over many identical nanostructures to be averaged [1], and by real-time magnetic imaging techniques, such as time-resolved photoemission on micron-sized structures [2]. Only recently, scanning probe techniques have been used for magnetization dynamics [3, 4] allowing researchers to measure magnetic excitations on the nanometer scale on individual structures. In all these cases, however, the accessible part of the magnon spectrum is restricted to the low energy part up to gigahertz frequencies, i.e. to the very bottom of the magnon spectrum with low energy and low momentum. To obtain a more complete view of the magnon spectrum, inelastic scattering techniques are required, which inherently do not give local information. Inelastic neutron scattering is the method of choice for bulk samples to probe the magnon spectrum away from the center of the Brillouin zone [5, 6]. Due to the low scattering cross section, the technique is ideal for bulk samples but not for thin films. For the latter, spin-polarized electron energy loss spectroscopy has been established as the standard tool due to the strong electron–magnon interaction caused by spin-flip or exchange scattering [7, 8]. This technique is most suitable for studying in-plane magnon dispersion, while the dispersion perpendicular to the film plane is hardly accessible [9]. We here focus on inelastic tunneling spectroscopy (ITS), which allows us to measure magnon energies on the local scale [10] and show that the dispersion perpendicular to the surface plane is accessible for fcc Mn, fcc Co and fcc Ni films on Cu_3Au or Cu(1 0 0).

A film is a two-dimensional system, i.e. magnons can freely propagate in the plane of the film leading to two-dimensional magnon bands. In the out-of-plane direction (z-axis), propagation is forbidden, and the film behaves like a quantum well for magnons. Due to the discrete nature of the system along the z-axis, i.e. there are N discrete atomic layers, N two-dimensional magnon bands form the spectrum (see figure 1(b)). To lowest order, calculating the magnon energies using a uniform nearest-neighbor Heisenberg model shows that at the $\bar{\Gamma}$ point, i.e. $q_{\parallel} = 0$, the discrete modes closely follow the original bulk dispersion (see figure 1(a)), if one assigns a

 © 2014 IOP Publishing Ltd Printed in the UK

TH-2014-36

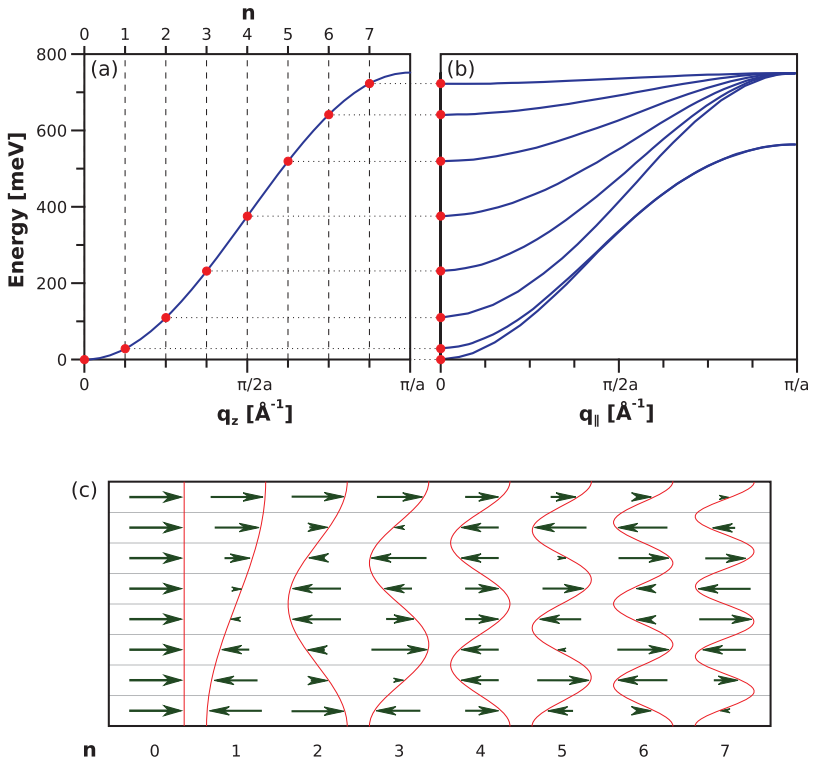

Figure 1. Magnon dispersion in an 8 ML thick Co film, calculated using the Heisenberg Hamiltonian. (*a*) The start of the bands at $q_\parallel = 0$ superimposed on the bulk dispersion. (*b*) The in-plane dispersion with eight bands. (*c*) The amplitude distribution in the z direction for the eight bands.

virtual wave vector to each mode in the form

$$q_n = \frac{n}{N} Q_{\max}, \quad n = 0, ..., N-1 \tag{1}$$

where $Q_{\max}$ is the Brillouin zone boundary in bulk for the z-axis direction. This corresponds to the standing modes of magnons being specularly reflected at both interfaces (see figure 1(*c*)). More elaborate calculations of the eigenmodes that go beyond this simple model require a treatment specific for the individual materials and film thicknesses and will be discussed below.

Inelastic excitation of these modes by tunneling electrons in ITS leads to peaks and dips in the second derivative of the tunneling current I with respect to the bias voltage U [10–12]. A peak in $\mathrm{d}^2I/\mathrm{d}U^2$ is produced when the energy of the tunneling electron (eU) reaches the energy of an inelastic excitation. A symmetric dip is produced at the negative bias of the same magnitude. For a magnon band, only low-$q_\parallel$ magnons contribute to the spectra [13], so the positions of the peaks and dips correspond to the band energy at $\bar{\Gamma}$. Therefore, we expect the inelastic spectra to have several peak–dip pairs, with the number of pairs depending on film thickness.

The ITS experiments were performed in two scanning tunneling microscopes at 4.2 K in an ultra-high vacuum ($p < 4 \times 10^{-11}$ mbar) with atomically clean samples and tips. The W tips were cleaned in vacuum by flashing, such that the end of the tips was melted. Cu_3Au and Cu(1 0 0) single crystals were cleaned by 3.0 kV Ar^+ sputtering and annealing such that Auger electron spectroscopy showed no contamination. Mn, Co and Ni films were deposited on the substrates at room temperature by electron beam evaporation from pure (99.99%) material. As the freshly deposited films of Co and Ni are relatively rough, they were annealed up to 370 K. This process was, however, not applied to the thinnest films, to avoid diffusion of Cu through the film [14]. Mn films showed flat terraces directly after deposition, such that no annealing step was necessary. The inelastic $\mathrm{d}^2I/\mathrm{d}U^2$ spectra were obtained by lock-in detection at 16.4 kHz and 5–10 meV modulation, and averaged over areas of some 100 nm^2.

The electronic and magnetic properties of the studied films were also investigated theoretically using a first-principles Green function method specially designed for layered semi-infinite systems [15]. The spin waves of the films were calculated using both the magnetic force theorem [16] and the linear response time-dependent density functional theory in the adiabatic local spin density approximation for dynamical magnetic susceptibility [17, 18]. The later theory offers the possibility of determining the lifetime of magnons.

1. Mn/Cu_3Au(1 0 0)

First, we review published experiments on Mn films illustrating the capability of the method [12]. Layer-wise antiferromagnetic Mn films, i.e. with parallel moments within the atomic layer and an antiparallel order between neighboring layers, have shown very pronounced inelastic features in an energy range of ±100 meV around the Fermi energy (see figure 2(*a*)). The spectra display up to three peak–dip pairs that shift to higher energies on lowering the film thickness, as expected for

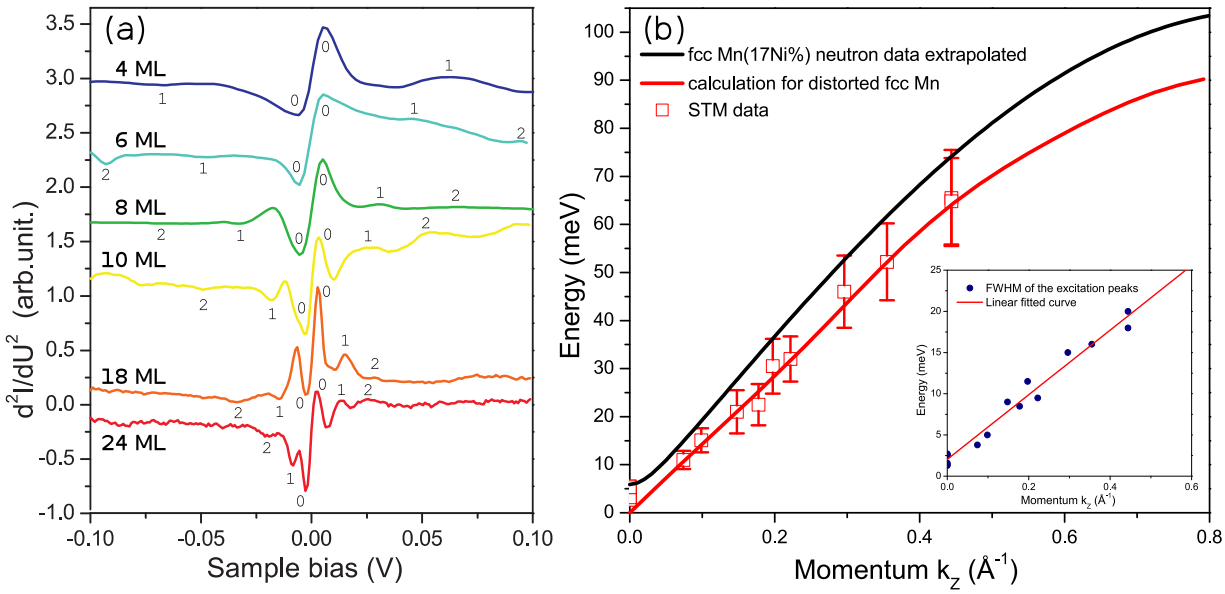

Figure 2. (*a*) Inelastic tunneling spectra recorded on Mn films with the thickness indicated. The inset shows the width of the excitation depending on the wave number. (*b*) Measured and calculated dispersion relations for magnons.

standing magnons. The peak–dip pairs were numbered starting from the Fermi level. The higher the order of the standing mode, the higher the energy and the stronger the inelastic features are broadened. The latter has been explained by a momentum (and thus energy) dependent damping in agreement with viscous damping [12]. This strong damping at high wave vectors broadens the peaks considerably, such that the inelastic features for higher wave vectors cannot be resolved. This is likely due to the selection rules for magnon excitation in antiferromagnets. While in ferromagnets only minority electrons tunneling into the ferromagnet can excite a magnon due to conservation of spin angular momentum [11], in layer-wise antiferromagnets electrons of both spins can excite magnons. This results on the one hand in a higher scattering cross section and thus stronger inelastic features, but on the other hand also means that the excited state can be de-excited with carriers of both spins reducing the lifetime of the excitations and thus increasing the broadening.

Using the above quantization for the wave vector, the dispersion has been reconstructed from the observed inelastic features displayed in figure 2(*b*). The constructed dispersion along the film normal closely follows the dispersion obtained on Ni-doped Mn samples by neutron scattering [19]. The doping is necessary to stabilize the fcc structure of Mn in the bulk. It agrees even better with *ab initio* calculations of tetragonally distorted fcc Mn, in which the experimental crystal structure of Mn films on $Cu_3Au(1\,0\,0)$ was used. This excellent agreement supports the interpretation of the inelastic features as magnons. Note that the relatively weak exchange produces magnons of energies well below 100 meV, which is an advantage for the interpretation of the ITS data. Within this low energy range, the local density of states (LDOS) in the Mn films is expected to vary only minutely, such that density of state effects play only a minor role in the $\mathrm{d}^2I/\mathrm{d}U^2$ spectra.

2. Co/Cu(1 0 0)

In ferromagnetic Co films, only minority electrons tunneling into the film can create magnons. At reversed bias, majority electrons tunneling from the film into the tip agree with the magnon creation selection rules [13]. Thus, we expect smaller inelastic features in the spectra compared to antiferromagnetic films. Furthermore, the damping of the excitations is expected to be less pronounced, such that high wave number excitations are more likely to show up in the spectra. As the exchange in Co is rather strong, the dispersion of magnons in Co spans a much wider energy interval, such that the inelastic spectra need to be taken over a larger energy range. As it is not reasonable to expect that the LDOS in Co films is constant over these energy ranges, we also expect fingerprints of the LDOS in the $\mathrm{d}^2I/\mathrm{d}U^2$ spectra, complicating the interpretation of the inelastic data.

The experimental $\mathrm{d}^2I/\mathrm{d}U^2$ curves, presented in figure 3(*a*), show a complicated peaked structure. As expected, the number of peaks scales with film thickness. The peak intensity decreases with the peak energy, while the width of the peak increases, indicating shorter magnon lifetimes at higher energies. This is expected due to the proximity of high energy modes to the Stoner continuum as well as to viscous damping. At the same time, the width of the peaks changes only slightly with film thickness, when comparing peaks in the same energy region. One also notices that all the spectra have a broad dip around −400 meV. For thin films (6 ML and 3.5 ML) this dip nearly completely hides the less intense structure expected for magnon excitations. Comparing the spectra with the band structure calculation and spin-resolved photoemission data for fcc Co on Cu(1 0 0), one can attribute this feature to a majority band edge, appearing at the same energy [20].

Knowing the energy of the excited magnons, we can construct the dispersion by assigning wave vectors to every peak according to (1). Note, however, that some of the peaks

do not come in pairs and are thus not related to magnetic excitations but to features in the density of states. Identified pairs are indicated in the figure.

Matching the peaks and dips proved to be successful for 9 ML and 7 ML thick films. For thinner films, the strong elastic feature in the negative part of the spectra totally hides the dips, so only the positive part of the spectra was used. Additional caution had to be exercised with the 3.5 ML film. As this film was not annealed after deposition to avoid intermixing [14], it exhibits small terraces (20 nm) of 3 ML and 4 ML local thicknesses. We can expect that if two areas of different thicknesses are mixed on such a short length scale, magnons will be excited with both sets of energies independent of the position. And indeed, the spectrum in figure 3(*a*) (3.5 ML) shows more than four peaks on the positive side. If we suppose that peaks on the positive side correspond to magnon modes in both 3 ML and 4 ML, we can construct two dispersions.

The magnon dispersion extracted from all the spectra for different thicknesses is collected in figure 3(*b*) and compared to the bulk dispersion going beyond nearest neighbors, calculated by Pajda *et al* [21]. Overall, the experiment shows that magnon dispersion in thin films closely follows the bulk dispersion down to 3 ML. The absolute values are, however, slightly lower than the calculations. Further, Bergqvist *et al* [22] and Costa *et al* [23] performed detailed calculations for Co/Cu(1 0 0) at specific film thicknesses. For comparison, we included the results of Bergqvist *et al* for 8 ML and 3 ML in our figure. Note that the 8 ML dispersion is close to the extrapolated bulk dispersion and the experimental data. The 3 ML modes are, however, at a much higher energy than the bulk dispersion, in contrast with the experimental data, which are lower. To compare our results with neutron scattering investigations, we calculated the spin-wave stiffness by fitting the lower part of the dispersion with a second-order polynomial. The resulting value of 360 ± 20 meV Å^2 is close to the previously reported values between 370 meV Å^2 and 450 meV Å^2 [6, 7, 24–27]. We can conclude that Co films on Cu(1 0 0) have an essentially bulk-like magnon dispersion normal to the plane, and the magnetism of the films is well described by a Heisenberg localized spin model. Note, however, that the dispersion of the thinner film lies systematically below that of the thicker. Although the reduction is small, it indicates the softening of magnons by finite-size effects. In contrast to the experimental observation of softening of the modes with decreasing film thickness, theoretical calculations indicate a hardening. This discrepancy can potentially be due to the adiabatic approximation in the calculations, which neglect mode softening due to relaxation by Stoner excitations in the non-magnetic Cu substrate (the spin pump effect) [18, 28]. Note that the observed features in the tunneling spectra do not agree with the dispersion of quantum well states in Co on Cu(1 0 0) [29].

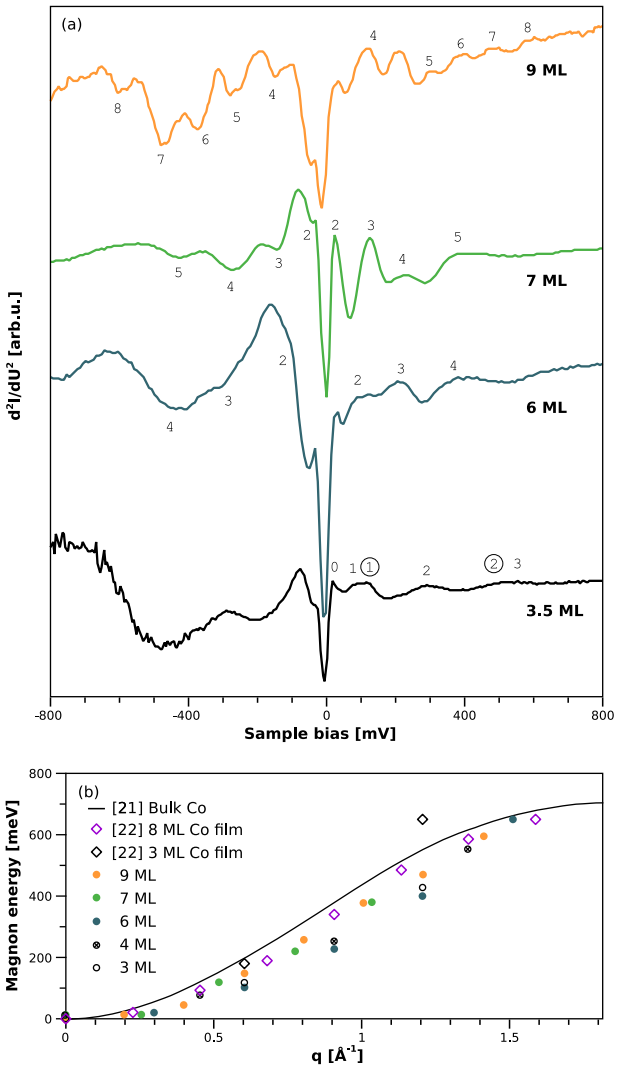

Figure 3. (*a*) $\mathrm{d}^2I/\mathrm{d}U^2$ measured on Co films of indicated thickness on Cu(1 0 0). The order of the sa standing magnon mode is indicated in the figure. For the 3.5 ML film, the circled indexes correspond to 3 ML and the non-circled to 4 ML. (*b*) The dispersion obtained from the experimental curves by matching peaks and dips for Co/Cu(1 0 0). The solid line is the dispersion obtained by Pajda *et al* for bulk fcc Co [21]. The open squares correspond to energies of the bands at the $\bar{\Gamma}$ point, calculated by Bergqvist *et al* [22].

3. Ni/Cu(1 0 0)

In contrast to Co, Ni is well known for the strong damping of magnons due to coupling to Stoner excitations, even at relatively low energies. Thus, we expect to see much broader inelastic features in the spectra, further complicating the evaluation of the experimental data.

The measurements, performed on Ni films 6, 8, 10 and 12 ML thick, show a behavior close to the one observed for Co (figure 4(*a*)), with the number of peaks scaling with film thickness. The width of the peaks has, however, a richer dependence on energy than for Co. This can well be attributed to a complex dependence of the damping on the wave vector, which has even been interpreted in bulk Ni neutron scattering as two intersecting magnon branches [5, 30] crossing at about 120 meV. This interpretation suggests that the Heisenberg picture of precessing rigid atomic moments is not operative for Ni, since this picture gives only one magnon mode for the systems with one magnetic atom per unit cell. Instead the complex properties of the multiple-band electronic structure must be taken into account.

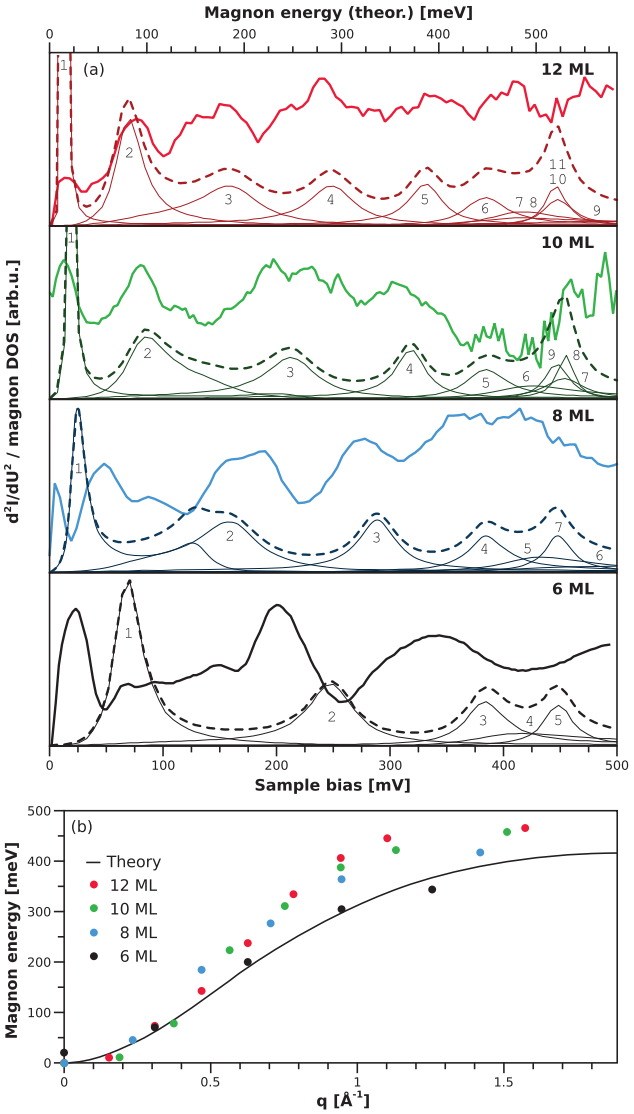

Figure 4. (*a*) $\mathrm{d}^2I/\mathrm{d}U^2$ (solid) measured for Ni films of indicated thickness on Cu(1 0 0) compared with the calculated magnon density of states (dashed) for Ni/Cu(1 0 0). The thin lines are the individual theoretically calculated magnon modes. (*b*) The dispersion obtained from the experimental curves by matching peaks and dips for Ni/Cu(1 0 0). The solid line is the dispersion obtained by Pajda *et al* for bulk fcc Ni [21].

Figure 4 shows the recorded inelastic spectra at positive bias as solid lines. By eye, it is rather difficult to assign individual inelastic peaks. The observed features are all rather broad except at energies below 100 meV, in agreement with the expectations from neutron scattering. Features in the density of states for Ni are less pronounced than for Co in the investigated energy region. However, the number of visible peaks is noticeably smaller than the number of layers. This can be partially attributed to strong damping. Thus, the inelastic tunneling data of Ni films cannot be directly used to construct a dispersion since the damping needs to be fully taken into account.

To explain the observed spectra, non-adiabatic *ab initio* calculations for Ni magnons were carried out. Since the calculations are very demanding, they were only performed for bulk Ni and the imaginary part of the susceptibility was evaluated at wave numbers corresponding to the standing magnon modes. The results of the theoretical calculations for the individual modes are indicated in the figure as thin solid lines. The lowest mode is not plotted, as the theoretically calculated energy is below our experimental energy resolution. Indeed, the damping is very pronounced, especially in the energy region between 100 meV and 250 meV and even more so for modes near the zone boundary. Also note that the dispersion is not monotonous. Maximal energies are found for wave vectors off the Brillouin zone boundary. In particular, these features are so broad that they nearly disappear. The dashed line is the sum of the expected inelastic signals, and for thick films reasonably corresponds to the observed spectrum. Note, however, that the calculated spectrum needed to be scaled down by 20% in energy. This issue is well known for Ni in *ab initio* calculations, which typically overestimate the exchange. The agreement between calculations and experiments gets worse for lower thicknesses. At 6 ML, the calculated peak positions are off the experimental ones by up to 50 meV.

With the help of the calculations, we identified the wave vector of the observed peaks and constructed a dispersion relation. The result, presented in figure 4(*b*), shows that Ni thickness has a much more pronounced influence on the dispersion than seen for Co. The top of the magnon band seems to be lower by about 100 meV for 6 ML of Ni compared to 10 ML. The spin-wave stiffness, calculated via a parabolic fit to the 12 ML and 10 ML dispersions up to $q = 0.6\,\text{Å}^{-1}$, has a value of 720 ± 20 meV Å^2. Comparison to an earlier theoretical calculation of magnon dispersion in bulk fcc Ni by Pajda *et al* [21] (solid line), shows that our energies are systematically higher than expected. The large discrepancy may mean one of two possibilities. The first is that our matching procedure for Ni is not acceptable and some of the peaks were missed during the evaluation leading to a general shift to lower q values and to a faster rising mode energy. As a second explanation, it might be possible that our results indicate a significant difference of the electronic structure between bulk fcc Ni and thin films of Ni/Cu(1 0 0) in the investigated film thickness region. A hint is provided by the double magnetization reorientation transition observed in Ni at higher temperatures for about 7 and about 40 ML [31], which exactly covers the region at which we observe elevated magnon energies, in part caused by the formation of dislocations in the Ni film. There is also strong disagreement between our dispersion and the results obtained by neutron scattering, which gives a spin wave stiffness of 400 ± 20 meV Å^2. Note, however, that the neutron scattering showed two branches and the value was extracted from only one branch.

4. Conclusions

In general, our research shows that ITS can be used to investigate magnon dispersion along the normal of thin films and to obtain information over the whole Brillouin zone, which is inaccessible by standard methods. A strong theoretical back-up is desirable to help distinguish magnon-related spectral features from background signals and the electron density of states. Such a back-up would be reliably provided by linear response theory.

Acknowledgments

The authors acknowledge funding by the DFG and discussions with the late D Mills.

References

[1] Tsai C C *et al* 2009 *Phys. Rev.* B **80** 014423
[2] Vogel J, Kuch W, Bonfim M, Camarero J, Pennec Y, Offi F, Fukomoto K, Kirschner J, Fontaine A and Pizzini S 2003 *Appl. Phys. Lett.* **82** 2299
[3] Züger O and Rugar D 1993 *Appl. Phys. Lett.* **63** 2496
[4] Meckenstock R 2008 *Rev. Sci. Instrum.* **79** 041101
[5] Mook H A and Paul D M 1985 *Phys. Rev. Lett.* **54** 227
[6] Liu X, Steiner M M, Sooryakumar R, Prinz G A, Farrow R F C and Harp G 1996 *Phys. Rev.* B **53** 12166
[7] Vollmer R, Etzkorn M, Kumar P S A, Ibach H and Kirschner J 2003 *Phys. Rev. Lett.* **91** 147201
[8] Rajeswari J, Ibach H, Schneider C, Costa A, Santos D and Mills D 2012 *Phys. Rev.* B **86** 165436
[9] Rajeswari J, Ibach H and Schneider C 2014 *Phys. Rev. Lett.* **112** 127202
[10] Heinrich A J, Gupta J A, Lutz C P and Eigler D M 2004 *Science* **306** 466
[11] Balashov T, Takács A F, Wulfhekel W and Kirschner J 2006 *Phys. Rev. Lett.* **97** 187201
[12] Gao C L, Ernst A, Fischer G, Hergert W, Bruno P, Wulfhekel W and Kirschner J 2008 *Phys. Rev. Lett.* **101** 167201
[13] Balashov T, Takács A F, Däne M, Ernst A, Bruno P and Wulfhekel W 2008 *Phys. Rev.* B **78** 174404
[14] Schmid A K, Atlan D, Itoh H, Heinrich B, Ichinokawa T and Kirschner J 1993 *Phys. Rev.* B **48** 2855
[15] Lüders M, Ernst A, Temmerman W M, Szotek Z and Durham P J 2001 *J. Phys.: Condens. Matter* **13** 8587
[16] Liechtenstein A I, Katsnelson M I, Antropov V P and Gubanov V A 1987 *J. Magn. Magn. Mater.* **67** 65
[17] Buczek P, Ernst A, Bruno P and Sandratskii L M 2009 *Phys. Rev. Lett.* **102** 247206
[18] Buczek P, Ernst A and Sandratskii L M 2011 *Phys. Rev.* B **84** 174418
[19] Jankowska-Kisielińska J, Mikke K and Milczarek J J 1995 *J. Magn. Magn. Mater.* **140–144** 1973
[20] Miyamoto K, Iori K, Sakamoto K, Kimura A, Qiao S, Shimada K, Namatame H and Taniguchi M 2008 *J. Phys.: Condens. Matter* **20** 225001
[21] Pajda M, Kudrnovský J, Turek I, Drchal V and Bruno P 2001 *Phys. Rev.* B **64** 174402
[22] Bergqvist L, Taroni A, Bergman A, Etz C and Eriksson O 2013 *Phys. Rev.* B **87** 144401
[23] Costa A, Muniz R and Mills D 2004 *Phys. Rev.* B **70** 054406
[24] Shirane G, Minkiewicz V J and Nathans R 1968 *J. Appl. Phys.* **39** 383
[25] Sinclair R N and Brockhouse B N 1960 *Phys. Rev.* **120** 1638
[26] Pickart S J, Alperin H A, Minkiewicz V J, Nathans R, Shirane G and Steinsvoll O 1967 *Phys. Rev.* **156** 623
[27] Vollmer R, Etzkorn M, Kumar P S A, Ibach H and Kirschner J 2004 *J. Appl. Phys.* **95** 7435
[28] Heinrich B, Burrowes C, Montoya E, Kardasz B, Girt E, Song Y Y, Sun Y and Wu M 2011 *Phys. Rev. Lett.* **107** 066604
[29] Ortega J E, Himpsel F J, Mankey G J and Willis R F 1993 *Phys. Rev.* B **47** 1540
[30] Cooke J F, Lynn J W and Davis H L 1980 *Phys. Rev.* B **21** 4118
[31] O'Brien W L, Droubay T and Tonner B P 1996 *Phys. Rev.* B **54** 9297